



Magmatism on rift flanks: insights from Ambient-Noise Phase-velocity in Afar region

Félicie Korostelev, Cornelis Weemstra, Sylvie Leroy, Lapo Boschi, Derek Keir,
Yong Ren, Irene Molinari, Abdulhakim Ahmed, Graham W. Stuart,
Frédérique Rolandone, et al.

► To cite this version:

Félicie Korostelev, Cornelis Weemstra, Sylvie Leroy, Lapo Boschi, Derek Keir, et al.. Magmatism on rift flanks: insights from Ambient-Noise Phase-velocity in Afar region. *Geophysical Research Letters*, 2015, 42 (7), pp.2179-2188. 10.1002/2015GL063259 . hal-01136108

HAL Id: hal-01136108

<https://hal.science/hal-01136108>

Submitted on 26 Mar 2015

HAL is a multi-disciplinary open access archive for the deposit and dissemination of scientific research documents, whether they are published or not. The documents may come from teaching and research institutions in France or abroad, or from public or private research centers.

L'archive ouverte pluridisciplinaire **HAL**, est destinée au dépôt et à la diffusion de documents scientifiques de niveau recherche, publiés ou non, émanant des établissements d'enseignement et de recherche français ou étrangers, des laboratoires publics ou privés.

**₁ Magmatism on rift flanks: insights from
₂ Ambient-Noise Phase-velocity in Afar region**

Félicie Korostelev,^{1,2} Cornelis Weemstra,³ Sylvie Leroy,^{1,2} Lapo Boschi^{1,2},
Derek Keir⁴, Yong Ren⁵, Irene Molinari⁶, Abdulhakim Ahmed^{1,2,7}, Graham
W. Stuart⁵, Frédérique Rolandone^{1,2}, Khaled Khanbari⁸, James O. S.
Hammond⁹, J. M. Kendall¹⁰, Cécile Doubre¹¹, Ismail Al Ganad¹², Berhe
Goitom¹³, and Atalay Ayele¹⁴

Corresponding author: Félicie Korostelev, (felicie.korostelev@gmail.com)

¹Sorbonne Universités, UPMC Univ Paris

During the breakup of continents in magmatic settings, the extension of the rift valley is commonly assumed to initially occur by border faulting and progressively migrate in space and time towards the spreading axis. Magmatic processes near the rift flanks are commonly ignored. We present phase-velocity maps of the crust and uppermost mantle of the conjugate margins of the southern Red Sea (Afar and Yemen) using ambient noise tomography to constrain crustal modification during breakup. Our images show that the low seismic velocities characterize not only the upper crust beneath the axial volcanic systems, but also both upper and lower crust beneath the rift flanks where ongoing volcanism and hydrothermal activity occur at the surface. Magmatic modification of the crust beneath rift flanks likely occurs for a protracted period of time during the breakup process, and may persist through to early seafloor spreading.

06, UMR 7193, Institut des Sciences de la

1. Introduction

During the breakup of continents, stretching and thinning of the plate commonly causes decompression melting and volcanism. In the resultant magmatically active rift valleys it is widely thought that extension is initially accommodated mainly by border faulting, and progressively localizes to relatively narrow axial volcanic segments as the rift valley widens [e.g. *Ebinger and Casey*, 2001]. However, it is becoming increasingly more recognized that magma intrusion and volcanism can occur on the rift flanks at an early stage of rifting [e.g. *Maccaferri et al.*, 2014]. These rift flank magmatic systems accommodate extension through diking [*Rooney et al.*, 2014], and thermally and compositionally modify the lithosphere [*Daniels et al.*, 2014]. Despite the importance of magmatic processes during continental extension, we have few constraints on their spatial and temporal variability. In order to address this issue we use ambient seismic noise tomography to image the Rayleigh wave phase-velocity structure of the crust in a region of late stage breakup at the conjugate margins of the southern Red Sea in Afar and Yemen.

Geochronological constraints in Ethiopia suggest rifting began 29-31 Ma on the western Afar margin [e.g. *Ayalew et al.*, 2006; *Wolfenden et al.*, 2005, Fig.1], approximately coeval with ~ 35 Ma faulting along large portions of the Gulf of Aden to the east [*Leroy et al.*, 2010]. Rifting was associated with the development of large offset border faults that currently define ~ 2000 - 3000 m of relief between the submarine Red Sea and subaerial Afar depression with the uplifted Ethiopian and Yemeni plateaus [*Wolfenden et al.*, 2004]. Extension is thought to have occurred above warm mantle with a potential temperature

Terre Paris (iSTeP), F-75005 Paris, France.

of ~ 1450 degrees [Rooney *et al.*, 2012], associated with voluminous flood basalts on the Ethiopian and Yemeni plateaus synchronous with the onset of extension [Wolfenden *et al.*, 2004], and associated with ongoing magmatism [Ferguson *et al.*, 2013]. At ~ 21 -23 Ma, magmatism occurred through dike intrusions along most of the eastern margin of the Red Sea [Bosworth *et al.*, 2005]. Magmatism on the rift flanks is ongoing, with the Quaternary to Recent volcanic centers of Sana'a, Dhamar and Marib located in Yemen [Manetti *et al.*, 1991; Korostelev *et al.*, 2014]. In addition, thermal hotspots are present along the conjugate southern Afar margin [Keir *et al.*, 2009]. Magma intrusion and volcanism is also common within the rift valley. Since ~ 10 Ma in Afar, extension via diking progressively localized to the rift axis [e.g. Wolfenden *et al.*, 2005; Rooney *et al.*, 2011], with the current locus of strain being ~ 70 -km-long, ~ 20 -km-wide axial volcanic segments such as the Dabbahu-Manda-Hararo segment in central-west Afar [e.g. Hayward and Ebinger, 1996]. Here, episodic intrusion of dikes fed from crustal magma chambers at both the segments centers and tips accommodates the majority of extension [e.g. Keir *et al.*, 2009; Grandin *et al.*, 2010, 2011].

Current opening across the kinematically complex southern Red Sea rift is constrained with relatively high-density GPS [e.g. ArRajehi *et al.*, 2010; McClusky *et al.*, 2010] and InSAR measurements [e.g. Pagli *et al.*, 2014]. These data show that south of $\sim 16^\circ\text{N}$, the rift bifurcates into two branches: the main Red Sea and the subaerial Red Sea rift in Afar (Danakil Depression). Partitioning of extension between rift branches varies along-strike.

²CNRS, UMR 7193, Institut des Sciences

North of $\sim 16^\circ\text{N}$, all the extension is accommodated in the main Red Sea rift, spreading at ~ 15 mm/yr. Moving south of 16°N , the extension is progressively accommodated in the Afar Depression reaching ~ 20 mm/yr at 13°N [McClusky *et al.*, 2010; Vigny *et al.*, 2006]. The crust beneath Afar varies from 25 km thick beneath most of Afar, to 15 km thick beneath the Danakil depression (Afdera-Erta’Ale segment) in the north [Makris and Ginzburg, 1987; Bastow and Keir, 2011, Fig.1]. The crustal thickness is ~ 25 km thick beneath the Danakil block and increases to 40-45 km beneath the Ethiopian and Yemeni Plateaus [Hammond *et al.*, 2011; Ahmed *et al.*, 2013, Fig.1].

2. Data

Our dataset is based on continuous recordings from 89 seismic stations. Only a limited number of high-quality permanent seismic stations span the Afar-southern Red Sea margins and so temporary experiments using portable broad-band equipment are our major source of information on the structure of the area. A seismic deployment was conducted between March 2009 and March 2010 as part of the YOCMAL (Young Conjugate Margins Laboratory) project, with 23 stations covering western Yemen during one year [Korostelev *et al.*, 2014; Corbeau *et al.*, 2014, Fig.2]. We also use data from 41 stations in the Afar Consortium network (UK and US, from March 2007 to November 2009) [e.g. Keir *et al.*, 2011], five stations of the Horn of Africa network in Yemen and Ethiopia [from June 1999 to December 2002, e.g. Sicilia *et al.*, 2008] and six temporary stations recording from May 2011 to September 2012 in Eritrea [e.g. Hammond *et al.*, 2013, Fig.2]. One station

de la Terre Paris (iSTeP), F-75005 Paris,

from the Djibouti temporary network was added to our dataset, together with permanent seismic stations in Djibouti, Yemen and Ethiopia.

The ambient-noise cross-correlation technique relies on having simultaneous recordings of the noise field at two seismic stations so that the Green's function between them can be estimated [Shapiro and Campillo, 2004; Wapenaar and Fokkema, 2006; Halliday and Curtis, 2008]. Because the different deployments of portable instruments occurred at different times, we are not able to estimate Green's functions for all receiver pairs. We partly compensate for this, however, by utilizing permanent stations from the IRIS and GEOSCOPE networks, providing data over a period during which several of the mentioned portable arrays were active.

3. Method

The ambient noise technique to study Earth structure is free of limitations imposed by the distribution of natural earthquakes. Extracting travel times from a multitude of station-station correlations therefore allows for relatively high-resolution tomographic inversions [e.g. Shapiro *et al.*, 2005]. We follow the approach of Ekström *et al.* [2009], discussed in further detail in section 3.2 of Boschi *et al.* [2013], to estimate phase velocity from the ambient signal recorded at two stations.

The background seismic noise is to a large extent generated by the coupling of oceans with the solid Earth [e.g. Longuet-Higgins, 1950; Hillers *et al.*, 2012]. Because this area is almost surrounded by seas or oceans (Red Sea, Gulf of Aden, Indian Ocean), it is particularly suitable for ambient noise surface wave retrieval.

France.

To maximize data quality, we (i) only used the pairs of stations that recorded simultaneously for at least 6 months, and (ii) compared measured and predicted Green's function for all station pairs, and discarded pairs that clearly showed a bad fit (see figure in supplementary material). The duration of cross-correlated signal varies by 6-36 months depending on the station pair. These long durations guarantee that all seasons and hence all possible azimuths of noise propagation are sampled [e.g. *Stehly et al.*, 2006]. Data processing was limited to whitening, as reasonable dispersion curves could be obtained without any filtering and/or "one-bit" amplitude compression.

4. Resolution

4.1. Station-to-station paths

To assess the resolving power of our inversion, we first show in Figure 2 the station-to-station paths corresponding to ambient Rayleigh-wave observations at each period. The solid gray line delimitates the area with good coverage, and therefore the zone of best resolution.

4.2. Random tests

We perform two random resolution tests [e.g. *Verbeke et al.*, 2012] to assess the reliability of the tomographic inversion: one with structures smaller than 100 km (Fig.3.a) and a second one with structures larger than 100 km (Fig.3.b). The input synthetic random

³Department of Geoscience and

velocity model consists of alternating random structures of opposite sign with a maximum velocity variation of 1.5% relative to the reference velocity.

Synthetic phase velocities were computed between the same station pairs as in the observed database. Figures 3.a and b show the input velocity models and the retrieved velocity models from these tests for periods of 9, 15.5 and 20.5 s. These synthetic tests indicate that our inversion can resolve most of the Afar-southern Red Sea margins region, with some degradation of the recovered solutions near the edges of the illuminated area. The tomography algorithm is that utilized e.g. by *Verbeke et al.* [2012]. Pixel-size is $0.1^\circ \times 0.1^\circ$.

Our synthetic tests (Fig.3) serve to validate both pixel size and select the values of regularization parameters that allow us to represent heterogeneities of scale-length such as in figure 3.a (left). The same parameterization and regularization is applied to real data in the following. Notice that resolution changes across the region of study, so that a unique resolution limit cannot be specified.

5. Results

We compute Rayleigh-wave phase-velocity maps for periods between 9 s and 25.5 s, and present examples at 9, 15.5 and 20.5 s (Fig.4; see supplementary material for other periods). According to e.g. *Lebedev and Van Der Hilst* [2008] and *Fry et al.* [2010], 9-s Rayleigh waves are most sensitive to depths < 20 km (upper and mid crust), while 15.5-s are most sensitive to 10 - 40 km depth (primarily the lower crust). 20.5-s Rayleigh waves can sample down to 70 km, at the top of the upper mantle. The locus of major

Engineering, Delft University of Technology,

velocity anomalies is fairly constant from 9 s to 15.5 s (Fig. 4). We image positive velocity perturbations beneath the border faults of the eastern flank of the Red Sea in Yemen, beneath the Danakil Horst, and in central western Afar in the region between the rift margin and the axial volcanic segments (Sullu Adu area, Fig.1). We also see positive velocity perturbations beneath the western Afar margin north of 12°N. The main slow anomalies are located beneath Dabbahu Manda-Hararo axial volcanic system, beneath Durrie off-axis volcano and the southern axis extension to Kurub volcano (Fig.1). We also find slow anomalies associated with the volcanic systems 150 to 200 km east of the rift margin in Yemen, and beneath the western Afar margin south of 12°N (Fig.4).

The magnitude of several of the distinct velocity perturbations varies subtly with period. For example, beneath the eastern rift margin (Tihama Plain, Yemen, Fig.1), the positive anomaly increases in magnitude from 5% at 9 s to 7% at 20.5 s (Fig. 4). The slow anomaly beneath the western Afar margin flank south of 12°N is mostly more than -3% at 9 s, whereas at 15.5 and 20.5 s a larger proportion of the anomaly is -4 to -6% (Fig.4).

The slow anomalies beneath Yemen and beneath the axial volcanic segment of Dabbahu-Manda-Hararo in Afar correlate well with the locus of surface volcanism (Fig.4). In addition, figure 5 shows the surface distribution of known thermal springs in the region [Keir *et al.*, 2009]. The slow anomaly beneath the western Afar margin is beneath the locus of thermal springs on the western Afar margin, whereas north of 12°N, thermal springs are absent and the crust is faster than average. The spatial extent of slow anomalies imaged

Stevinweg 1, 2628 CN Delft, The

using ambient noise also correlates well with the spatial extent of high V_p/V_s ratios in the crust constrained using P-S receiver functions [*Hammond et al.*, 2011].

6. Discussion

Seismic wave velocity is known to be affected by the temperature and chemical composition of the medium of propagation (crustal rocks), as well as by the concentration of fluids, such as partial melt that might be present within crustal rocks [e.g. *Christensen and Mooney*, 1995; *Karato et al.*, 2003]. We image slow velocities beneath axial regions of localized magma intrusion, consistent with the hypothesis that major surface-wave slow anomalies are associated with magmatism (Fig.4). In addition, the lowest velocities in our images are beneath zones of active volcanism and geothermal activity near the flanks of the southern Red Sea conjugate margins (Fig. 4 and 5). The magnitude of the anomalies and spatial association with regions where either partial melt or fluids released from cooling magmatic systems are present suggests the crust beneath the flanks of the rift is currently being modified by magmatic processes. Ongoing magmatism occurs at the rift flanks in spite of the majority of strain having shifted to the rift axis since the onset of rifting at 11 Ma [*Wolfenden et al.*, 2004]. Beneath the western Afar margin, where slow anomalies are associated with geothermal systems rather than known volcanoes, geological studies suggest early border faulting at 30 Ma was associated with spatially localized volcanism in the marginal graben systems [*Ayalew et al.*, 2006]. Our velocity maps suggest that the magmatic systems beneath the rift flanks that were active during the onset of rifting, remain magmatically active throughout the breakup process either through con-

Netherlands.

tinued minor accumulation of partial melt in reservoirs, dike intrusion, and / or ongoing
 conductive cooling leading to release of fluids such as water [Keir *et al.*, 2009; Holtzman
et al., 2010].

The low-velocity anomalies in our phase-velocity maps under the rift axis are observed
 with higher amplitude in the upper crust (Fig.4, period = 9 seconds), whereas the low-
 velocity anomalies located beneath the rift flanks are observed both in the upper and
 lower crust, but with higher amplitude in the lower crust (Fig.4, period = 15.5 seconds).
 This is consistent with the proposed plumbing systems of axial and flank volcanic systems
 of the nearby Main Ethiopian Rift, where petrological constraints on flank volcanism are
 good. The volcanic products observed on the flanks and at the axis of the MER are not
 identical: they consist mainly of trachytes for the flanks, and mainly of rhyolites and
 basalts for the axis [Peccerillo *et al.*, 2007]. Petrological models indicate that the origin of
 the off-axis trachytes is probably high-pressure fractional crystallization of asthenosphere-
 derived basalts, with this fractionation occurring at the base of the crust [Peccerillo *et al.*,
 2007]. Rooney *et al.* [2005, 2007] suggest that these off-axis volcanic products result of
 moderate-degree partial melting at 50-90 km depth and undergo fractional crystalliza-
 tion in complex plumbing systems spanning depths throughout the crust [Rooney *et al.*,
 2011]. The volcanic rocks at the axis are asthenospheric basalts produced by rift-related
 decompressional melting, rather than other potential sources such as melting in the crust.
 The axial basalts undergo fractional crystallization mostly in the upper crust [Peccerillo

⁴National Oceanography Centre

et al., 2007]. Thus, the axial magmatic chamber is shallow (in the upper crust), and the melt ascension from the asthenosphere is probably rapid. At the flanks, however, there is a complex plumbing system with stacked-reservoirs both in the upper and lower crust [Rooney *et al.*, 2011]. The geothermal systems of the flanks are probably fed or heated by such a complex plumbing system (Fig.5). Our surface-wave velocity maps are consistent with this model and therefore suggest similar magmatic plumbing systems for the southernmost Red Sea.

According to Medynski *et al.* [2015], the magma supply has decreased in the Dabbahu-Manda-Hararo axis reservoir since 15 kyr. An off-axis reservoir, located 15 km to the west of the Dabbahu-Manda-Hararo rift beneath Durrie volcano has been actively fed since 15 kyr, and is currently imaged using magneto-telluric techniques (Fig.1) [Desissa *et al.*, 2013]. It is consistent with our phase-velocity maps, where the maximum amplitude for the northern Dabbahu-Manda-Hararo seems to be slightly to the west of the rift, beneath Durrie volcano (Fig.4).

In the past, geodynamic models of breakup ignored the presence and impact of maintained magmatism at rift flanks on the thermal and subsidence history of the rift during late stage breakup and early seafloor spreading. At the southern Red Sea, where seafloor spreading is young, our new crustal-velocity maps coupled with surface expression of volcanism (Fig.4) show clear evidence for ongoing magmatism beneath the rift flanks in Afar and Yemen (Sana'a, Dhamar and Marib volcanic fields, Fig.1) [Korostelev *et al.*, 2014; Corbeau *et al.*, 2014]. Similarly, there is evidence for ongoing dike intrusion further north

Southampton, University of Southampton,

211 along the eastern Red Sea flank from InSAR (interferometric synthetic aperture radar)
 212 and seismicity studies at Harrat Lunayyir volcanic system in Saudi Arabia [e.g. *Pallister*
 213 *et al.*, 2010; *Ebinger et al.*, 2010]. There, localized subsidence, horizontal opening and
 214 earthquakes in April to May 2009 are best modeled by intrusion of a dike and induced
 215 normal faulting. These studies, combined with the evidence presented by our new surface-
 216 wave velocity maps, demonstrate that rift flank magmatism during late stage breakup may
 217 be more common than previously assumed.

7. Conclusions

218 Our study provides new high-resolution phase-velocity maps of the crust and uppermost
 219 mantle of the conjugate margins of the southern Red Sea (Afar and Yemen) using ambient
 220 noise tomography to constrain crustal evolution during breakup. Low-velocity anomalies
 221 are imaged in the crust beneath the axial volcanic systems, but also in the upper and
 222 lower crust beneath rift flanks where hydrothermal activity and ongoing volcanism are
 223 observed at the surface. Our results show that the crust beneath the southern Red sea
 224 rift flanks is currently being modified by magmatic processes, and that this activity is
 225 continuous from the onset of rifting. We therefore demonstrate that rift flank magmatism
 226 after breakup may be more common than it was previously thought in context of margins
 227 with excess magmatism.

228 **Acknowledgments.** This project was funded by the ANR-07-BLAN-0135 YOCMAL,
 229 CNRS-INSU-PICS Yemen, GSMRB Yemen and is in the framework of the Actions

Southampton, SO14 3ZH, U.K.

Marges program. Seismic equipment from SEIS-UK is funded by NERC under agreement R8/H10/64. We thank David Hawthorn, Alex Brisbane and Victoria Lane for their efforts during the deployment and servicing of network, the French Embassy in Yemen, local governors and the people of the Yemen governorates for their help during the field work. The authors thank Raphael Pik, Nicolas Bellahsen and Martin Stab for discussions about the Afar region. DK is supported by NERC grant NE/L013932/1. CW is supported by the Netherlands Research Centre for Integrated Solid Earth Science (ISES). Djibouti instruments belong to the French national pool of portable seismic instruments Sismob-RESIF and IPGS/EOST (University of Strasbourg).

References

- Ahmed, A., C. Tiberi, S. Leroy, G. W. Stuart, D. Keir, J. Sholan, K. Khanbari, I. Al-Ganad, and C. Basuyau (2013), Crustal structure of the rifted volcanic margins and uplifted plateau of Western Yemen from receiver function analysis, *Geophysical Journal International*, 193(3), 1673–1690.
- ArRajehi, A., S. McClusky, R. Reilinger, M. Daoud, A. Alchalbi, S. Ergintav, F. Gomez, J. Sholan, F. Bou-Rabee, G. Ogubazghi, et al. (2010), Geodetic constraints on present-day motion of the Arabian Plate: Implications for Red sea and Gulf of Aden rifting, *Tectonics*, 29(3), TC3011.

⁵School of Earth and Environment,

- 247 Ayalew, D., C. Ebinger, E. Bourdon, E. Wolfenden, G. Yirgu, and N. Grassineau (2006),
248 Temporal compositional variation of syn-rift rhyolites along the western margin of the
249 southern Red Sea and northern Main Ethiopian Rift, *Geological Society, London, Special*
250 *Publications*, 259(1), 121–130.
- 251 Bastow, I. D., and D. Keir (2011), The protracted development of the continent-ocean
252 transition in Afar, *Nature Geoscience*, 4(4), 248–250.
- 253 Boschi, L., C. Weemstra, J. Verbeke, G. Ekström, A. Zunino, and D. Giardini (2013), On
254 measuring surface wave phase velocity from station–station cross-correlation of ambient
255 signal, *Geophysical Journal International*, 192(1), 346–358.
- 256 Bosworth, W., P. Huchon, and K. McClay (2005), The Red Sea and Gulf of Aden Basins,
257 *Journal of African Earth Sciences*, 43(1-3), 334–378.
- 258 Christensen, N. I., and W. D. Mooney (1995), Seismic velocity structure and composition
259 of the continental crust: A global view, *Journal of Geophysical Research: Solid Earth*
260 (1978–2012), 100(B6), 9761–9788.
- 261 Corbeau, J., F. Rolandone, S. Leroy, A. Al-Lazki, D. Keir, G. Stuart, and A. Stork (2014),
262 Uppermost mantle velocity from Pn tomography in the Gulf of Aden, *Geosphere*.
- 263 Daniels, K., I. Bastow, D. Keir, R. Sparks, and T. Menand (2014), Thermal models of
264 dyke intrusion during development of continent–ocean transition, *Earth and Planetary*
265 *Science Letters*, 385, 145–153.
- 266 Desissa, M., N. Johnson, K. Whaler, S. Hautot, S. Fisseha, and G. Dawes (2013), A
267 mantle magma reservoir beneath an incipient mid-ocean ridge in Afar, Ethiopia, *Nature*

University of Leeds, Leeds, U.K.

geoscience, 6(10), 861–865.

Drake, C. L., and R. Girdler (1964), A geophysical study of the Red Sea, *Geophysical Journal International*, 8(5), 473–495.

Ebinger, C., and M. Casey (2001), Continental breakup in magmatic provinces: An Ethiopian example, *Geology*, 29(6), 527–530.

Ebinger, C., D. Keir, A. Ayele, E. Calais, T. Wright, M. Belachew, J. Hammond, E. Campbell, and W. Buck (2008), Capturing magma intrusion and faulting processes during continental rupture: seismicity of the Dabbahu (Afar) rift, *Geophysical Journal International*, 174(3), 1138–1152.

Ebinger, C., A. Ayele, D. Keir, J. Rowland, G. Yirgu, T. Wright, M. Belachew, and I. Hamling (2010), Length and timescales of rift faulting and magma intrusion: the Afar rifting cycle from 2005 to present, *Annual Review of Earth and Planetary Sciences*, 38, 439–466.

Egloff, F., R. Rihm, J. Makris, Y. Izzeldin, M. Bobsien, K. Meier, P. Junge, T. Noman, and W. Warsi (1991), Contrasting structural styles of the eastern and western margins of the southern Red Sea: the 1988 SONNE experiment, *Tectonophysics*, 198(2), 329–353.

Ekström, G., G. A. Abers, and S. C. Webb (2009), Determination of surface-wave phase velocities across USArray from noise and Aki’s spectral formulation, *Geophysical Research Letters*, 36(18), L18,301.

⁶Istituto Nazionale di Geofisica e

287 Ferguson, D. J., J. MacLennan, I. Bastow, D. Pyle, S. Jones, D. Keir, J. Blundy, T. Plank,
288 and G. Yirgu (2013), Melting during late-stage rifting in Afar is hot and deep, *Nature*,

Vulcanologia, via di Vigna Murata 605,
00143 Roma, Italy.

⁷Seismological and Volcanological
Observatory Center, Dhamar, Yemen.

⁸Sana'a University, Yemen Remote
Sensing and GIS Center, Sana'a, Yemen.

⁹Imperial College London, London, SW7,
U.K.

¹⁰University of Bristol, Bristol, BS8, U.K.

¹¹Institut de Physique du Globe de
Strasbourg; UMR 7516, Université de
Strasbourg/EOST, CNRS, 5 rue René
Descartes, F-67084 Strasbourg Cedex.

¹²Yemen Geological Survey and mineral
Resources Board, Sana'a, Yemen.

¹³School of Earth Sciences, University of
Bristol, Bristol, UK.

¹⁴Institute of Geophysics, Space Science
and Astronomy, Addis Ababa University.

499(7456), 70–73.

Fry, B., F. Deschamps, E. Kissling, L. Stehly, and D. Giardini (2010), Layered azimuthal anisotropy of Rayleigh wave phase velocities in the European Alpine lithosphere inferred from ambient noise, *Earth and Planetary Science Letters*, 297(1), 95–102.

Grandin, R., A. Socquet, E. Jacques, N. Mazzoni, J.-B. de Chabalier, and G. King (2010), Sequence of rifting in Afar, Manda-Hararo rift, Ethiopia, 2005–2009: Time-space evolution and interactions between dikes from interferometric synthetic aperture radar and static stress change modeling, *Journal of Geophysical Research: Solid Earth* (1978–2012), 115(B10).

Grandin, R., E. Jacques, A. Nercessian, A. Ayele, C. Doubre, A. Socquet, D. Keir, M. Kasim, A. Lemarchand, and G. King (2011), Seismicity during lateral dike propagation: Insights from new data in the recent Manda Hararo–Dabbahu rifting episode (Afar, Ethiopia), *Geochemistry, Geophysics, Geosystems*, 12(4).

Halliday, D., and A. Curtis (2008), Seismic interferometry, surface waves and source distribution, *Geophysical Journal International*, 175(3), 1067–1087.

Hammond, J., J.-M. Kendall, G. Stuart, D. Keir, C. Ebinger, A. Ayele, and M. Belachew (2011), The nature of the crust beneath the Afar triple junction: evidence from receiver functions, *Geochemistry, Geophysics, Geosystems*, 12(12).

Hammond, J., J.-M. Kendall, G. Stuart, C. Ebinger, I. Bastow, D. Keir, A. Ayele, M. Belachew, B. Goitom, G. Ogubazghi, and T. Wright (2013), Mantle upwelling and initiation of rift segmentation beneath the Afar Depression, *Geology*, 41(6), 635–638.

- 310 Hayward, N., and C. Ebinger (1996), Variations in the along-axis segmentation of the
311 Afar Rift system, *Tectonics*, 15(2), 244–257.
- 312 Hillers, G., N. Graham, M. Campillo, S. Kedar, M. Landès, and N. Shapiro (2012),
313 Global oceanic microseism sources as seen by seismic arrays and predicted by wave
314 action models, *Geochemistry, Geophysics, Geosystems*, 13(1).
- 315 Holtzman, B. K., J. Kendall, et al. (2010), Organized melt, seismic anisotropy, and plate
316 boundary lubrication, *Geochemistry, Geophysics, Geosystems*, 11(12).
- 317 Karato, S. i., et al. (2003), *The dynamic structure of the deep earth: an interdisciplinary*
318 *approach*, Princeton University Press.
- 319 Keir, D., I. Bastow, K. Whaler, E. Daly, D. Cornwell, and S. Hautot (2009), Lower crustal
320 earthquakes near the Ethiopian rift induced by magmatic processes, *Geochem. Geophys.*
321 *Geosyst*, 10(10).
- 322 Keir, D., C. Pagli, I. Bastow, and A. Ayele (2011), The magma-assisted removal of Arabia
323 in Afar: Evidence from dike injection in the Ethiopian rift captured using InSAR and
324 seismicity, *Tectonics*, 30(2), TC2008.
- 325 Korostelev, F., C. Basuyau, S. Leroy, C. Tiberi, A. Ahmed, G. W. Stuart, D. Keir,
326 F. Rolandone, I. Ganad, K. Khanbari, et al. (2014), Crustal and upper mantle structure
327 beneath south-western margin of the arabian peninsula from teleseismic tomography,
328 *Geochemistry, Geophysics, Geosystems*, 15(7), 2850–2864.
- 329 Laughton, A., and C. Tramontini (1969), Recent studies of the crustal structure in the
330 Gulf of Aden, *Tectonophysics*, 8(4), 359–375.

- 331 Lebedev, S., and R. D. Van Der Hilst (2008), Global upper-mantle tomography with
332 the automated multimode inversion of surface and S-wave forms, *Geophysical Journal*
333 *International*, *173*(2), 505–518.
- 334 Leroy, S., F. Lucazeau, E. d’Acremont, L. Watremez, J. Autin, S. Rouzo, N. Bellahsen,
335 C. Tiberi, C. Ebinger, M. Beslier, et al. (2010), Contrasted styles of rifting in the
336 eastern Gulf of Aden: A combined wide-angle, multichannel seismic, and heat flow
337 survey, *Geochemistry Geophysics Geosystems*, *11*(7), Q07,004.
- 338 Longuet-Higgins, M. S. (1950), A theory of the origin of microseisms, *Philosophical Trans-*
339 *actions of the Royal Society of London. Series A, Mathematical and Physical Sciences*,
340 *243*(857), 1–35.
- 341 Maccaferri, F., E. Rivalta, D. Keir, and V. Acocella (2014), Off-rift volcanism in rift zones
342 determined by crustal unloading, *Nature Geoscience*.
- 343 Makris, J., and A. Ginzburg (1987), The Afar Depression: transition between continental
344 rifting and sea-floor spreading, *Tectonophysics*, *141*(1), 199–214.
- 345 Manetti, P., G. Capaldi, S. Chiesa, L. Civetta, S. Conticelli, M. Gasparon, L. Volpe,
346 and G. Orsi (1991), Magmatism of the eastern Red Sea margin in the northern part of
347 Yemen from Oligocene to present, *Tectonophysics*, *198*(2), 181–202.
- 348 McClusky, S., R. Reilinger, G. Ogubazghi, A. Amleson, B. Healeb, P. Vernant, J. Sholan,
349 S. Fisseha, L. Asfaw, R. Bendick, et al. (2010), Kinematics of the southern Red Sea–Afar
350 Triple Junction and implications for plate dynamics, *Geophys. Res. Lett.*, *37*, L05,301.
- 351 Medynski, S., R. Pik, P. Burnard, C. Vye-Brown, L. France, I. Schimmelpfennig,
352 K. Whaler, N. Johnson, L. Benedetti, D. Ayelew, et al. (2015), Stability of rift axis

magma reservoirs: Spatial and temporal evolution of magma supply in the dabbahu rift segment (afar, ethiopia) over the past 30 kyr, *Earth and Planetary Science Letters*, 409, 278–289.

Pagli, C., H. Wang, T. J. Wright, E. Calais, and E. Lewi (2014), Current plate boundary deformation of the Afar rift from a 3-D velocity field inversion of InSAR and GPS, *Journal of Geophysical Research: Solid Earth*, 119(11), 8562–8575.

Pallister, J., W. McCausland, S. Jónsson, Z. Lu, H. Zahran, S. El Hadidy, A. Aburukbah, I. Stewart, P. Lundgren, R. White, et al. (2010), Broad accommodation of rift-related extension recorded by dyke intrusion in Saudi Arabia, *Nature Geoscience*, 3(10), 705–712.

Peccerillo, A., C. Donati, A. Santo, A. Orlando, G. Yirgu, and D. Ayalew (2007), Petrogenesis of silicic peralkaline rocks in the Ethiopian rift: geochemical evidence and volcanological implications, *Journal of African Earth Sciences*, 48(2), 161–173.

Prodehl, C., and J. Mechie (1991), Crustal thinning in relationship to the evolution of the Afro-Arabian rift system: a review of seismic-refraction data, *Tectonophysics*, 198(2), 311–327.

Reed, C. A., S. Almadani, S. S. Gao, A. A. Elsheikh, S. Cherie, M. G. Abdelsalam, A. K. Thurmond, and K. H. Liu (2014), Receiver function constraints on crustal seismic velocities and partial melting beneath the Red Sea rift and adjacent regions, Afar Depression, *Journal of Geophysical Research: Solid Earth*, 119(3), 2138–2152.

Rooney, T., T. Furman, I. Bastow, D. Ayalew, and G. Yirgu (2007), Lithospheric modification during crustal extension in the Main Ethiopian Rift, *J. Geophys. Res.*, 112,

B10,201.

Rooney, T., I. Bastow, and D. Keir (2011), Insights into extensional processes during magma assisted rifting: Evidence from aligned scoria cones, *Journal of Volcanology and Geothermal Research*, 201(1-4), 83–96.

Rooney, T., C. Herzberg, and I. Bastow (2012), Elevated mantle temperature beneath East Africa, *Geology*, 40(1), 27–30.

Rooney, T. O., T. Furman, G. Yirgu, and D. Ayalew (2005), Structure of the Ethiopian lithosphere: Xenolith evidence in the Main Ethiopian Rift, *Geochimica et Cosmochimica Acta*, 69(15), 3889–3910.

Rooney, T. O., I. D. Bastow, D. Keir, F. Mazzarini, E. Movsesian, E. B. Grosfils, J. R. Zimbelman, M. S. Ramsey, D. Ayalew, and G. Yirgu (2014), The protracted development of focused magmatic intrusion during continental rifting, *Tectonics*.

Ruegg, J. (1975), Main results about the crustal and upper mantle structure of the Djibouti region (TFAI), *Afar Depression of Ethiopia*, 1, 120–134.

Shapiro, N. M., and M. Campillo (2004), Emergence of broadband Rayleigh waves from correlations of the ambient seismic noise, *Geophysical Research Letters*, 31(7).

Shapiro, N. M., M. Campillo, L. Stehly, and M. H. Ritzwoller (2005), High-resolution surface-wave tomography from ambient seismic noise, *Science*, 307(5715), 1615–1618.

Sicilia, D., J. Montagner, M. Cara, E. Stutzmann, E. Debayle, J. Lépine, J. Lévêque, E. Beucler, A. Sebai, G. Roult, et al. (2008), Upper mantle structure of shear-waves velocities and stratification of anisotropy in the Afar Hotspot region, *Tectonophysics*, 462(1-4), 164–177.

397 Stab, M., N. Bellahsen, R. Pik, S. Leroy, and D. Ayalew (2014), Mode of rifting in
398 magmatic-rich setting: Tectono-magmatic evolution of the central afar rift system, in
399 *EGU General Assembly Conference Abstracts*, vol. 16, p. 14484.

400 Stehly, L., M. Campillo, and N. Shapiro (2006), A study of the seismic noise from its long-
401 range correlation properties, *Journal of Geophysical Research: Solid Earth (1978–2012)*,
402 111(B10).

403 Tramontini, C., and D. Davies (1969), A seismic refraction survey in the Red Sea, *Geo-
404 physical Journal International*, 17(2), 225–241.

405 Verbeke, J., L. Boschi, L. Stehly, E. Kissling, and A. Michelini (2012), High-resolution
406 Rayleigh-wave velocity maps of central Europe from a dense ambient-noise data set,
407 *Geophysical Journal International*, 188(3), 1173–1187.

408 Vigny, C., P. Huchon, J.-C. Ruegg, K. Khanbari, and L. M. Asfaw (2006), Confirmation of
409 Arabia plate slow motion by new GPS data in Yemen, *Journal of Geophysical Research:
410 Solid Earth (1978–2012)*, 111(B2).

411 Wapenaar, K., and J. Fokkema (2006), Green’s function representations for seismic inter-
412 ferometry, *Geophysics*, 71(4), SI33–SI46.

413 Wolfenden, E., C. Ebinger, G. Yirgu, A. Deino, and D. Ayalew (2004), Evolution of the
414 northern Main Ethiopian rift: birth of a triple junction, *Earth and Planetary Science
415 Letters*, 224(1), 213–228.

416 Wolfenden, E., C. Ebinger, G. Yirgu, P. Renne, and S. Kelley (2005), Evolution of a
417 volcanic rifted margin: Southern Red Sea, Ethiopia, *Geological Society of America
418 Bulletin*, 117(7-8), 846–864.

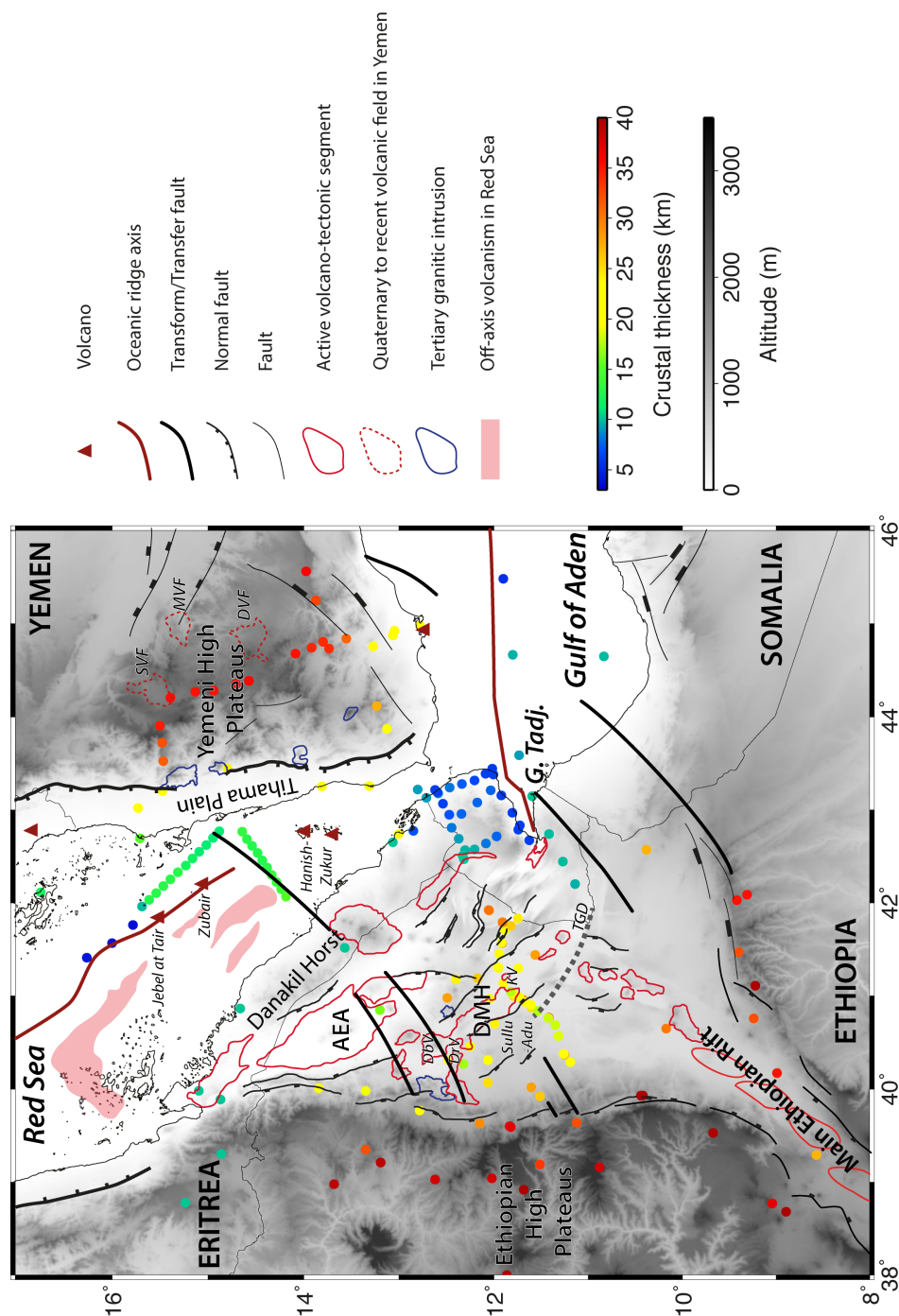


Figure 1. Structure of the Afar and southern Red Sea region. The crustal thicknesses are displayed by colored dots and based on the Moho depths, which are obtained from *Egloff et al.* [1991]; *Tramontini and Davies* [1969]; *Drake and Girdler* [1964]; *Prodehl and Mechie* [1991]; *Laughton and Tramontini* [1969]; *Ruegg* [1975]; *Hammond et al.* [2011]; *Ahmed et al.* [2013]; *Reed et al.* [2014]. Structures are modified from *Ebinger et al.* [2008] and *Stab et al.* [2014]. Bathymetry is not represented. DMH: Dabbahu-Manda-Hararo volcano-tectonic segment; AEA: Afdera-Erta’Ale volcano-tectonic segment; G. Tadj.: Gulf of Tadjura; DbV: Dabbahu volcano; DrV: Durrie volcano; KV: Kurub volcano; TGD: Tendaho-Goba’ad Discontinuity; SVF: Sana’a volcanic field; MVF: Marib volcanic field; DVF: Dhamar volcanic field.

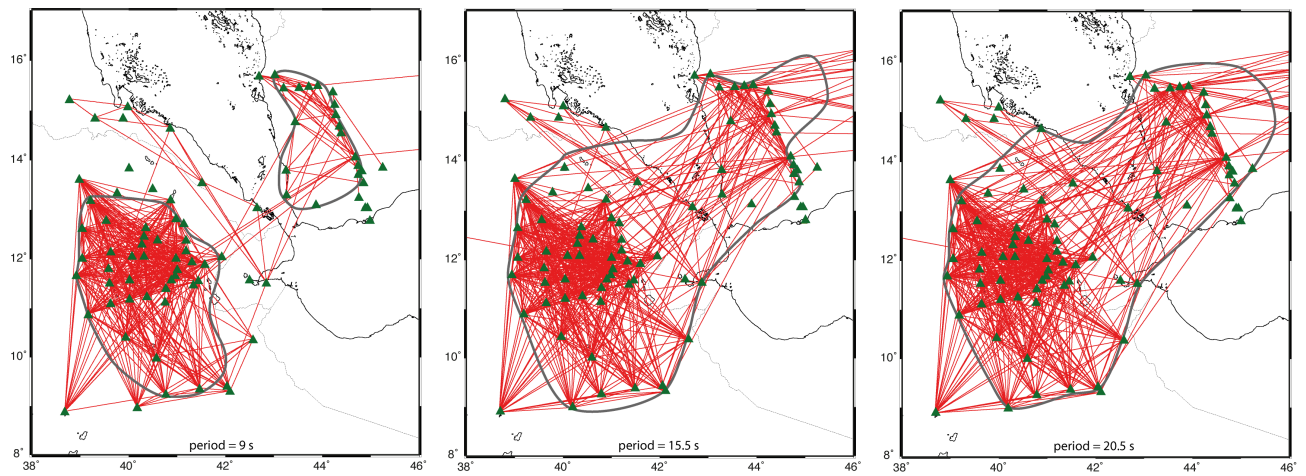


Figure 2. Map of the station pairs used for the tomographic inversion. The red lines show the station-to-station paths. The solid gray line delimitates the best constrained area. The green triangles are the stations.

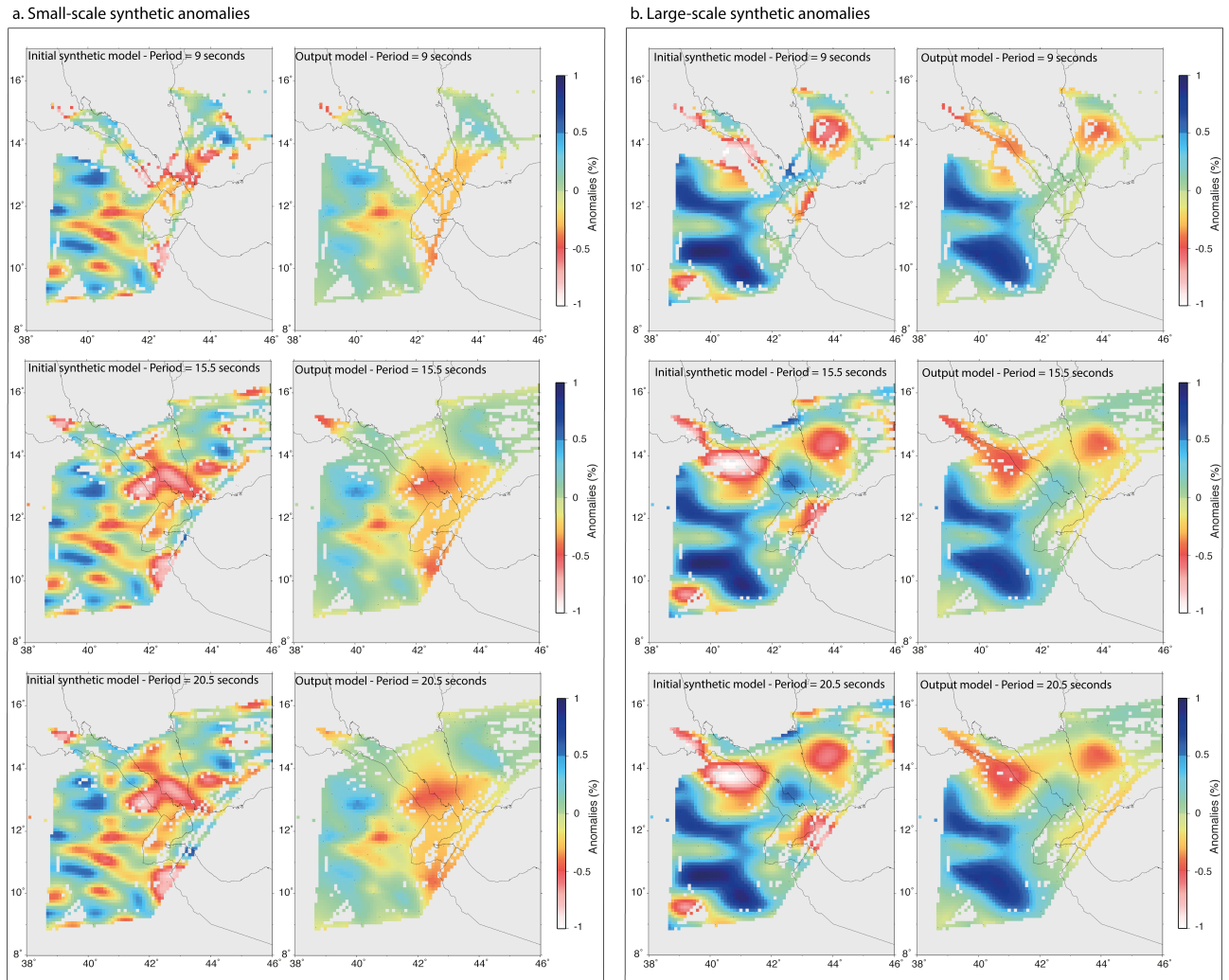


Figure 3. Result of two reconstruction synthetic tests with randomly distributed velocity anomalies of various size as input. a. Small-scale synthetic anomalies; b. large-scale synthetic anomalies. The left image displays the synthetic input, whereas the right image displays the output model.

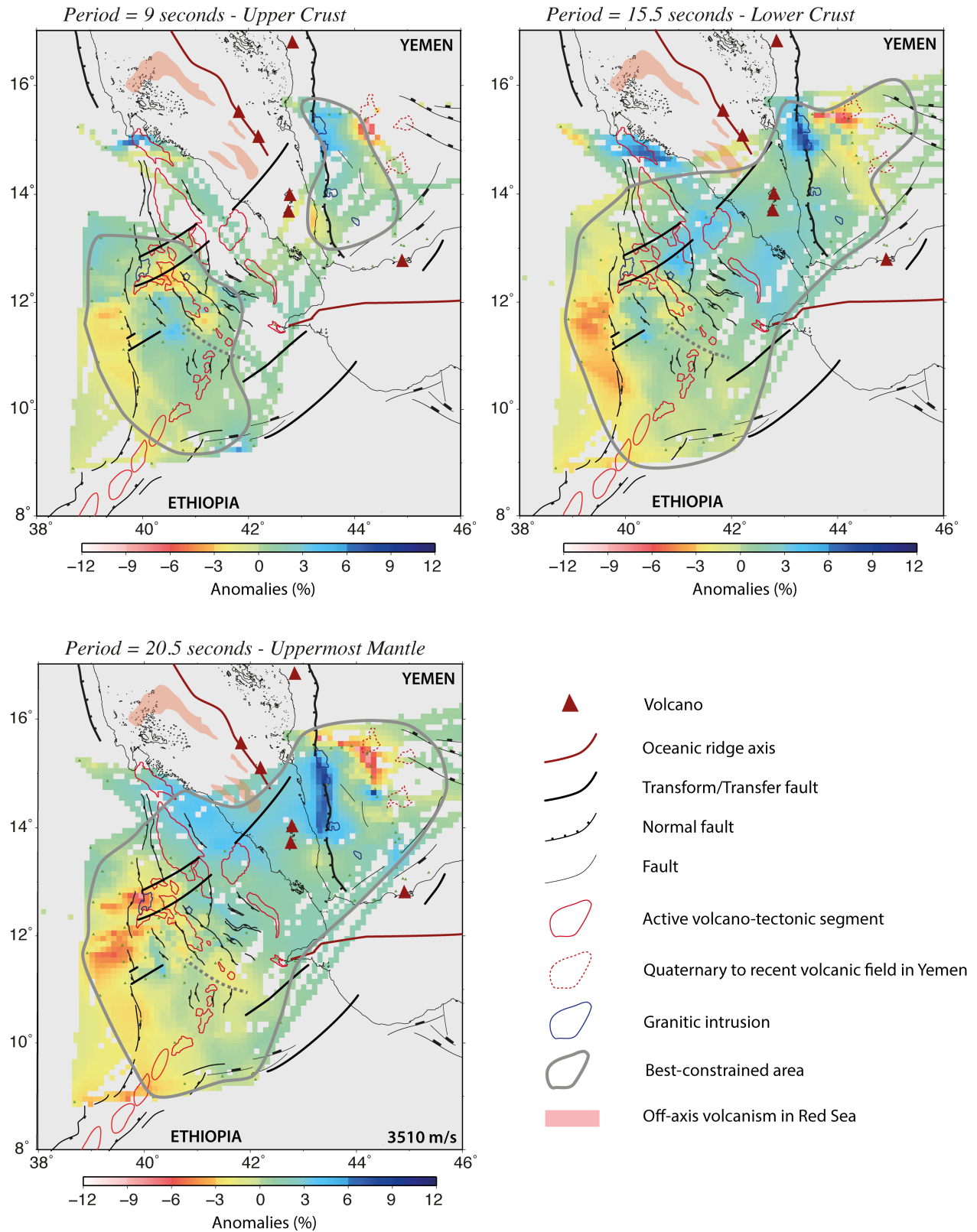


Figure 4. Maps of phase velocity anomalies (%) with respect to average) resulting from tomographic inversion of ambient noise dispersion data. The average velocity for each period is 3510 m/s. The color scale indicates the phase velocity anomalies. The maps show the distribution of phase velocity anomalies across the Red Sea region, with the best-constrained area highlighted in gray. The velocity scale is 3510 m/s. The maps are labeled YEMEN and ETHIOPIA. The legend identifies the following features: Volcano (Red triangle), Oceanic ridge axis (Red line), Transform/Transfer fault (Black line), Normal fault (Black line), Fault (Black line), Active volcano-tectonic segment (Red outline), Quaternary to recent volcanic field in Yemen (Red outline), Granitic intrusion (Blue outline), Best-constrained area (Gray outline), Off-axis volcanism in Red Sea (Pink area).

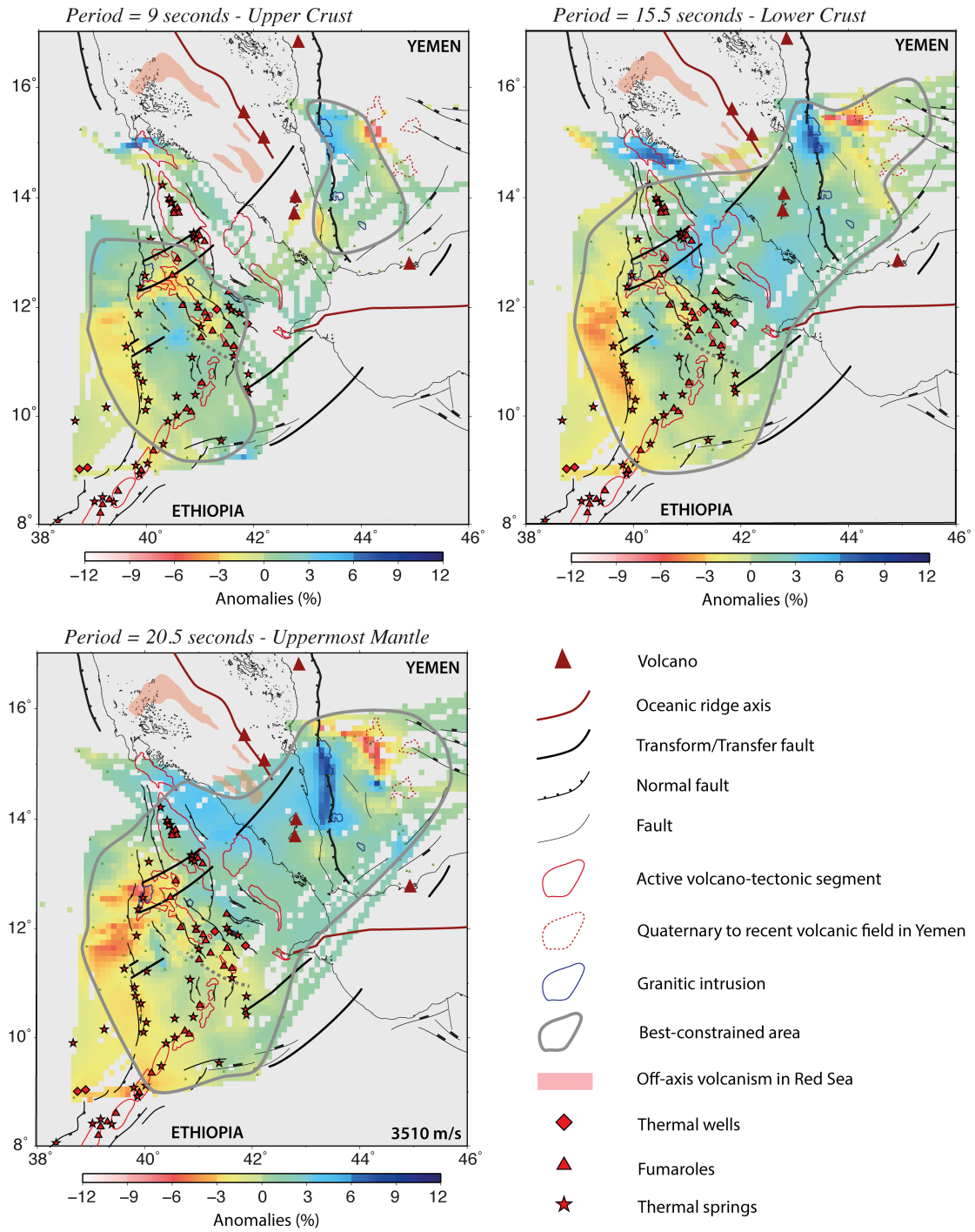


Figure 5. Distribution of thermal wells, fumaroles and thermal springs in the Afar triple junction region [Keir *et al.*, 2009]. No data was available in Yemen. The green triangles are the stations.